Research Article | Vol. 28, No. 2 / 20 January 2020 / Optics Express 1426
Optics EXPRESS

Engineering novel tunable optical high-Q nanoparticle array filters for a wide range of wavelengths

A. D. Utyushev,[1,2,3] I. L. Isaev,[3] V. S. Gerasimov,[1,3,4] A. E. Ershov,[1,2,3,4] V. I. Zakomirnyi,[1,4,5,6] I. L. Rasskazov,[7] S. P. Polyutov,[1,6] H. Ågren,[4,5] and S. V. Karpov[1,2,4,6,*]

[1]Siberian Federal University, Krasnoyarsk 660041, Russia
[2]Siberian State University of Science and Technology, 660014 Krasnoyarsk, Russia
[3]Institute of Computational Modeling, Federal Research Center KSC SB RAS, 660036 Krasnoyarsk, Russia
[4]Federal Siberian Research Clinical Center under FMBA of Russia, Krasnoyarsk 660037, Russia
[5]Division of Theoretical Chemistry and Biology, Royal Institute of Technology, SE-100 44 Stockholm, Sweden
[6]Kirensky Institute of Physics, Federal Research Center KSC SB RAS, 660036 Krasnoyarsk, Russia
[7]The Institute of Optics, University of Rochester, Rochester, NY 14627, USA
*karpov@iph.krasn.ru

Abstract: The interaction of non-monochromatic radiation with arrays comprising plasmonic and dielectric nanoparticles has been studied using the finite-difference time-domain electrodynamics method. It is shown that $LiNbO_3$, TiO_2, GaAs, Si, and Ge all-dielectric nanoparticle arrays can provide a complete selective reflection of an incident plane wave within a narrow spectral line of collective lattice resonance with a Q-factor of 10^3 or larger at various spectral ranges, while plasmonic refractory TiN and chemically stable Au nanoparticle arrays provide high-Q resonances with moderate reflectivity. Arrays with fixed dimensional parameters make it possible to fine-tune the position of a selected resonant spectral line by tilting the array relative to the direction of the incident radiation. These effects provide grounds for engineering novel selective tunable optical high-Q filters in a wide range of wavelengths, from visible to middle-IR.

1. Introduction

Design and fabrication of new compact optical elements with high-Q response in the visible, near infrared (IR), and middle-IR wavelength ranges is a research topic in applied optics with high priority and wide ramifications. Much attention has been focused on devices in the form of periodic one-dimensional (1D) or two-dimensional (2D) arrays composed of plasmonic or all-dielectric nanoparticles (NPs) with Mie resonance. New ideas underlying such devices stem from the effect first predicted in theoretical and experimental studies of rough surfaces [1] and particle gratings [2] further extended for regular plasmonic structures [3–8]. According to these predictions, periodic arrays of NPs with strong electromagnetic coupling are capable to support high-Q collective lattice resonances (CLRs) with the Fano type profile in extinction spectra due to the interaction of fields of individual particles and the Wood-Rayleigh anomaly [9,10]. In the general case, the lattice resonance arises in periodic arrays in which the phase of the external field of a plane wave in the vicinity of an individual array element coincides with the phase of the field produced by neighboring elements. If such coherence takes place within the entire array at a given wavelength, a resonance excitation occurs at this wavelength. Thus, resonance excitation is produced by the hybrid coupling of localized low Q-factor resonances of NPs and their non-localized interactions covering the entire array. The spectral position and Q-factor of these resonances depend on the geometry of the array lattice, the material composition and the

#380922 https://doi.org/10.1364/OE.28.001426
Journal © 2020 Received 20 Oct 2019; revised 28 Nov 2019; accepted 28 Nov 2019; published 9 Jan 2020

Optics EXPRESS

shape of the NPs. Under particular conditions, the Q-factor of such resonances can exceed the Q-factor of a single NP by 10^2–10^3 times.

CLRs in periodic arrays of plasmonic [11–15] and all-dielectric [16–24] NPs have been extensively discussed during the recent decade owing to the great number of potential applications in color printing [25–28], biosensing [29–32], lasing [33,34], fluorescence enhancement [35] and etc [36,37]. Light transmission through 2D subwavelength hole arrays in perfect-conductor films and the reflection on same array of nonabsorbing scatterers was shown to be complete at same wavelength of CLR in the dipole approximation in [38,39]. In [40–43], CLRs were observed in the arrays of Si NPs with Q-factor values from 20 to several hundreds. Note that in all-dielectric systems mainly silicon is used for fabricating nanoparticle arrays. In this regard, the relevance of the analysis of materials suitable for fabricating such arrays is obvious, since a certain material with its optical constants is best suited for each spectral range. In addition, an analysis and optimization of the dimensional characteristics of arrays are needed for a significant increase of the CLR Q-factors.

The goal of our paper is to verify the relevance of the concept of CLRs for solving applied problems and the advantages they can offer. Within the frame of this goal we propose the design of a device that makes it possible to select radiation in the reflection mode from the spectral continuum within a tunable ultra-narrow spectral line and to control its position with a high Q-factor. Data on the optimal structure of the device – particle size and shape – lattice period and a particle material are obtained to achieve this goal.

2. Methods

We consider 2D arrays of nanodisks (NDs) with height H and radius R arranged in a regular square lattice with period h, as shown in Fig. 1(a). The arrays are embedded in a homogeneous environment with refractive index n_m = 1.45, which corresponds to quartz in the spectral range under study. Such structures can be fabricated using a lithography technique on a quartz substrate and subsequent sputtering a layer of quartz on top of the array. A homogeneous environment is an important factor in the model, because the Q-factor of CLR drops dramatically in the case of the half-space geometry, where the substrate and the superstrate have different refractive indices [44]. The reflection spectra of such structures are calculated with a commercial Finite-Difference Time-Domain (FDTD) method software [45]. FDTD is a widely used computational method of electrodynamics, which in general shows excellent agreement with experimental results for CLRs [7,14,43,46]. The optical response of the infinite array is simulated by considering a single particle unit cell with periodic boundary conditions applied at the lateral boundaries of the simulation box and perfectly matched layers (PML) used at the remaining top and bottom sides, as shown in Fig. 1(b). Arrays are illuminated from the top by plane waves with normal incidence along the Z axis and polarization along the Y axis. The reflection has been calculated

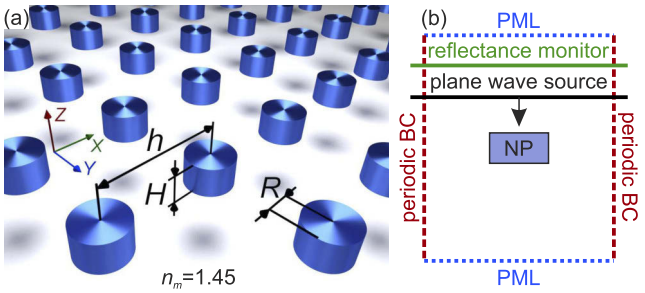

Fig. 1. (a) Sketch of the NDs array under consideration; (b) FDTD simulation setup.

Optics EXPRESS

at the top of the simulation box using a discrete Fourier transform monitor which is placed above the plane-wave source. The angular dependencies were obtained using the broadband fixed angle source technique [47]. An adaptive mesh has been used to reproduce accurately the nanodisk shape. Finally, extensive convergence tests for each set of parameters have been performed to avoid undesired reflections on the PMLs.

We study arrays of both plasmonic (TiN and Au) and all-dielectric ($LiNbO_3$, TiO_2, Si, GaAs, Ge) nanoparticles. Figure 2 shows tabulated experimental data for the real and imaginary parts of the complex refractive index n which have been used for each material.

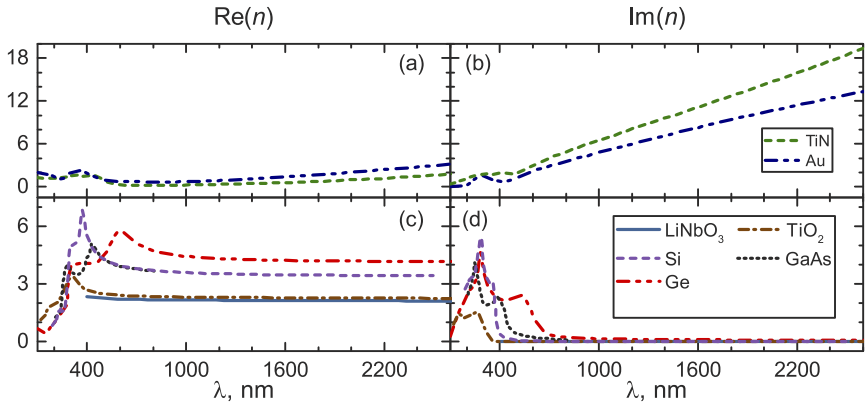

Fig. 2. Real and imaginary parts of complex refractive index n for (a) and (b) plasmonic TiN [48] and Au [49]; (c) and (d) all-dielectric $LiNbO_3$ [50] (here we consider only ordinary refractive index), TiO_2 [51], GaAs [52], Si [53] and Ge [54].

3. Results

The lattice period h varies in accordance with Rayleigh anomalies $(\pm 1, 0)$ and $(0, \pm 1)$, the positions of which for the case of normal incidence and homogeneous environment with refractive index n_m are defined as

$$\lambda_{p,q} = hn_m / \sqrt{p^2 + q^2}\,, \tag{1}$$

where λ is the vacuum wavelength, p and q are integers which represent the phase difference (in 2π units) between waves scattered by two adjacent elements of the array and incident wave in the x and y directions. Equation (1) describes the condition of constructive interference for particles within the XOY plane [55].

Before discussing CLRs in NP arrays we note that the shape of the NPs is an important parameter that affects the Q-factor of the CLRs. In the calculations we examined two types of the NP shapes: nanodisks and nanoparallelepipeds. Both shapes can be simply experimentally fabricated [41,43]. We found that nanodisks demonstrate slightly higher value of Q-factors compared to nanoparallelepipeds, so that the further studies were carried out only with nanodisks.

3.1. Reflection spectra of plasmonic nanoparticle arrays

Plasmonic nanoparticle arrays were the first type of structures used for observation of CLRs with the Fano-type profile [3–5]. Au is a widely used material in these arrays for which the CLRs are observed in the red range of the visible spectrum [6–8]. The use of TiN ND arrays provides moderate reflectivity with a high Q-factor of CLRs in the telecommunication spectral range, as shown in Fig. 3. The optimal TiN ND radius is 90 nm. A larger particle size results in a decrease of the reflectivity and Q-factor. Figure 3 shows that Au ND arrays exhibit CLRs in the

Optics EXPRESS

long-wavelength part of the visible and near-IR ranges with reflectivity about twice as much as for TiN, though, with a lower Q-factor. The suppression of surface plasmon resonances in classic plasmonic materials under extreme conditions [56–58] may result in a reduction of the Q-factor and CLR amplitude. The use of refractory TiN alleviates this problem, keeping quite high values of Q-factor even for heated NDs [15], which is advantageous for using arrays exhibiting CLRs at high temperatures.

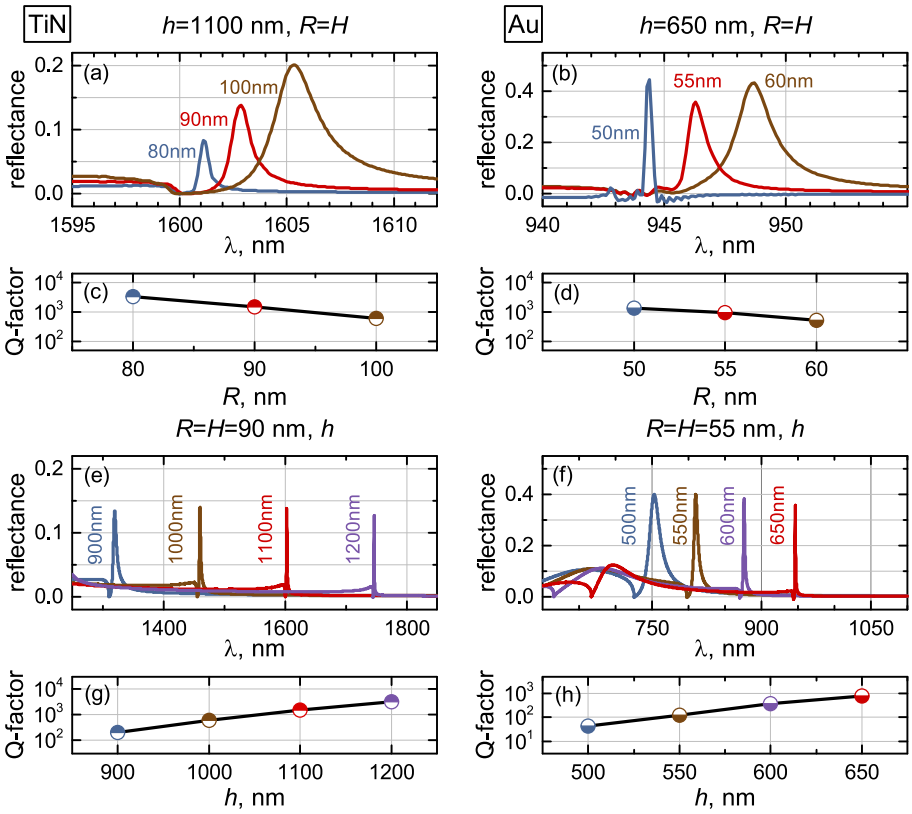

Fig. 3. Reflection spectra for TiN (left) and Au (right) ND arrays with: (a) fixed h = 1100 nm, and for different $R = H$ as shown in legend; (b) fixed h = 650 nm, and for different $R = H$ as shown in legend; (c) and (d) corresponding quality factors of CLRs; (e) fixed $R = H$ = 90 nm and for different h as shown in legend; (f) fixed $R = H$ = 55 nm and for different h as shown in legend; (g) and (h) corresponding quality factors of CLRs.

3.2. Dielectric nanoparticle arrays

3.2.1. Reflection spectra

In the case of dielectric nanoparticle structures the main intrinsic property which makes them attractive refers to the combination of high real part of the refractive index Re(n) and a low imaginary part Im(n) for different spectral ranges which ensures low absorption inside the particles. Figures 2(c) and 2(d) show, in particular, the refractive indices of the following suitable lossless materials satisfying these requirements: $LiNbO_3$, TiO_2, Si, GaAs, Ge. In this paper we have selected materials for each spectral range to obtain high-Q CLR in each given case. Two materials were chosen for the visible spectral range: $LiNbO_3$ and TiO_2.

Optics EXPRESS

First of all, we begin by discussing the general features regarding CLRs in arrays of dielectric nanoparticles. We should note that in arrays with large dielectric particles with a size of tens of nanometers and above, the conditions arise for the appearance of a magnetic dipole resonance along with an electric dipole excitation. The geometric parameters of the array such as period, size and shape of nanoparticles significantly affect the position of electric and magnetic dipole resonances and enable to suppress the magnetic dipole resonance as well as to prevent the appearance of several close lines in the spectrum instead of a single line which is unacceptable for selective narrow-band filters in the tuning spectral range.

Studies of the radiation reflection from NP arrays call for a clarification of what type of resonance excitation is associated with reflection and what is its origin. Figure 4(a) shows two overlapping spectral lines in the reflection spectrum of the $LiNbO_3$ ND array associated with the excitation of both electric dipole and magnetic dipole CLRs. Different values of the lattice periods used in the calculations make it possible to detect the appearance of a magnetic dipole resonance in the reflection spectrum separately from the electric dipole excitation band. For instance, Figs. 4(b)–4(g) show the configuration of electric and magnetic fields in orthogonal planes inside a unit cell for the wavelength $\lambda = 365$ nm Figs. 4(b) and 4(e), for $\lambda = 370$ nm Figs. 4(c) and 4(f), and for $\lambda = 474$ nm Figs. 4(d) and 4(g). We can see that at $\lambda = 365$ nm, the field configuration corresponds to the magnetic dipole along X axis while at $\lambda = 370$ nm and $\lambda = 474$ nm it is typical for electric dipole along Y axis (see also [41,42,59]). Calculations for all

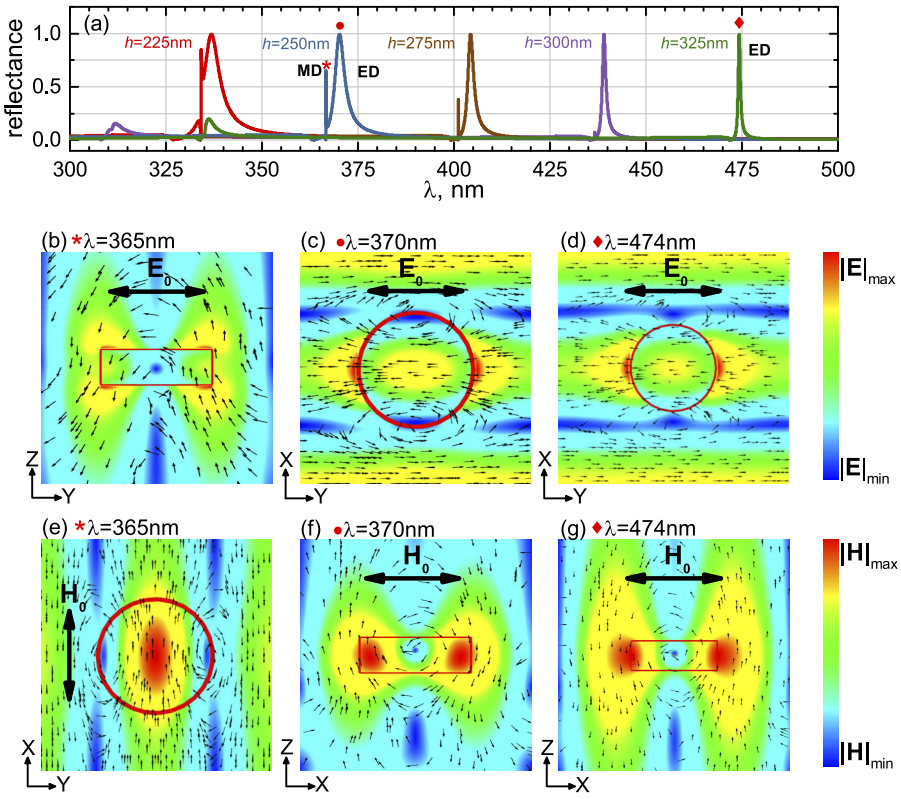

Fig. 4. (a) Reflection spectra of the $LiNbO_3$ ND arrays with $R = H = 60$ nm for different lattice period h (shown in legend), (b), (e) configurations of the electric and magnetic fields at $\lambda = 365$ nm (the period $h = 250$ nm); (c), (f) configurations for $\lambda = 370$ nm (the period $h = 250$ nm); (d), (g) configurations for period $h = 325$ nm at $\lambda = 474$ nm.

Optics EXPRESS

subsequent spectra in the paper were also preceded by an analysis of CLRs to confirm its electric dipole nature.

The effect of the aspect ratio (R/H) of the NDs on the obtained dependencies is of particular interest. We look for maximum values of the reflection coefficient in combination with high Q-factors of the CLRs provided by an optimal value of the particle aspect ratio R/H which in our case is close to 1. The results in Fig. 5 demonstrate that for a fixed value of the particle radius R = 60 nm and a decrease in $R/H<1$ due to the growing particle height H, the Q-factor starts to decrease while the reflection coefficient remains equal to 1. This is accompanied by a red CLR shift. When $R/H>1$ by reducing the height, the Q-factor is growing, but at the same time the reflection coefficient decreases. In this case we observe a blue CLR shift. At a fixed height H = 60 nm, an increase in the radius in aspect ratio $R/H>1$ results in a drop in the Q-factor and a red shift of CLR while maintaining the reflection coefficient equal to 1. A decrease in the radius in $R/H<1$ is accompanied by an increase in the Q-factor and a simultaneous fall in the reflection coefficient with a blue CLR shift.

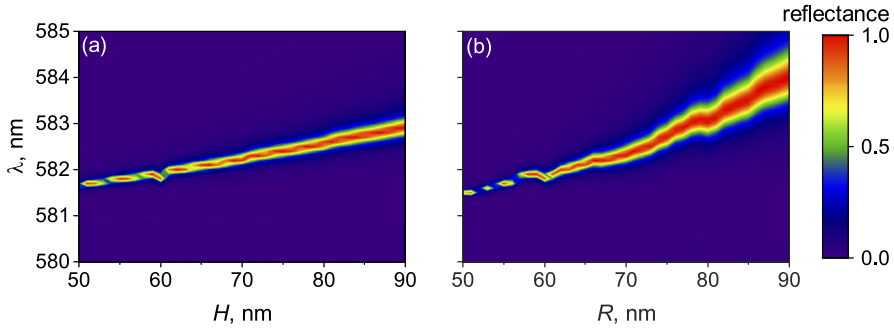

Fig. 5. Dependencies of the reflection spectra of the $LiNbO_3$ ND array with period h = 400 nm on a ND aspect ratio: (a) variation of the ND height H at R = 60 nm, (b) variation of the ND radius R at H = 60 nm.

Figures 6(a)–6(d) with reflection spectra of $LiNbO_3$ and TiO_2 ND arrays show that the larger the particle size, the lower the Q-factor, but at the same time the higher the reflection coefficient. So the optimal combination of these factor gives a particle radius of 60 nm with a Q-factor equal to 10^3. Figures 6(c)–6(d) and 6(g)–6(h) show that employing these materials in ND arrays provides ultra-narrowband resonances in the entire visible range with a Q-factor over 10^3 and high reflection. The utilization of TiO_2 in ND arrays also provides high reflectivity and Q-factor, however, with smaller size of the particle – 50 nm compared to $LiNbO_3$ that results in narrowing the spectral range with high reflectivity, see Fig. 6. The next step is to vary the lattice period with the given optimal radius. Calculations show that the Q-factor of the CLR increases with wavelength.

The best materials for the near-IR range are Si and GaAs. These materials in the IR range demonstrate the properties of dielectrics (Fig. 2) with a near-zero imaginary part of the refractive index and its high real part, which makes it possible to excite Mie resonances in such particles with radius below 100 nm – much smaller than the wavelength. Figure 7 shows the reflection spectra of Si ND arrays with ND radii R = 100, 110, and 120 nm and radius/height ratio R/H = 1. Besides that, Fig. 7 shows that CLRs with reflected radiation appear in the entire telecommunication wavelength range by varying the array period. In [43] authors experimentally studied CLRs in near-IR range in the reflection mode in Si ND arrays with Q-factor equals 300 – 10 for ND aspect ratio 2.4 – 3.78 and H = 100 nm. As follows from Fig. 7, the ND parameters used in [43] could not provide higher Q-factor because of too large particle sizes and non-optimal aspect ratio R/H

Optics EXPRESS

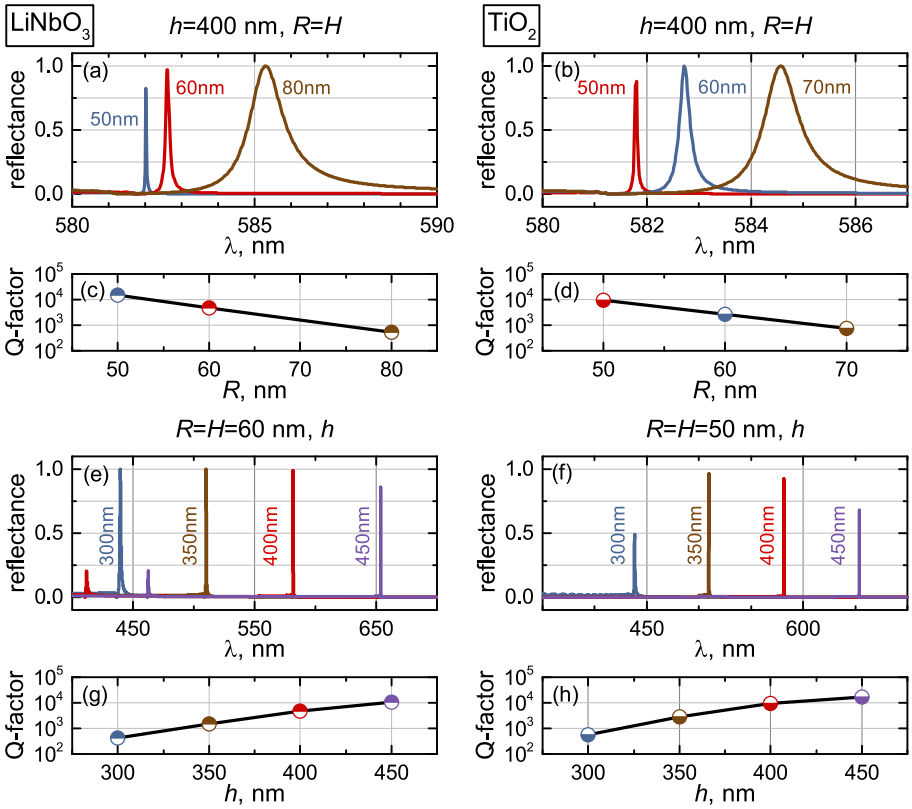

Fig. 6. Reflection spectra for $LiNbO_3$ (left) and TiO_2 (right) ND arrays with: (a) and (b) fixed h = 400 nm and different $R = H$ as shown in legend; (c) and (d) corresponding quality factors of CLRs; (e) fixed $R = H$ = 60 nm and for different h as shown in legend; (f) fixed $R = H$ = 50 nm and for different h as shown in legend; (g) and (h) corresponding quality factors of CLRs.

over 3 instead of 1. Figure 7 shows that Q-factor can be much higher for considered parameters of arrays.

Reflection spectra for GaAs ND arrays have optimal characteristics in the range between visible and telecom wavelengths (Fig. 7). The optimal ND radius equals 70 nm and period 600–700 nm with an ultrahigh Q-factor.

The use of the Ge ND arrays provides high reflectivity and Q-factor in the middle-IR range with optimal ND radius 165 nm. A smaller size of the particle results in a decrease of reflectivity, larger ones are accompanied by lower Q-factors (Fig. 8).

Besides, we note one more important feature of the CLRs in the studied arrays, namely that minor array defects, that may occur during their experimental fabrication, do not significantly affect the Q-factor of the CLRs [60].

3.2.2. Scale invariance of collective lattice resonances

Arrays of all-dielectric NPs demonstrate an important feature in conditions of utilizing materials with zero dispersion: the spectral position of CLR in NP arrays as all-dielectric systems can be predicted by multiplying all dimensional parameters of the array (particle radius, height and lattice period) by the same number K. The new resonance position will correspond to $K\lambda$ (where λ is the previous wavelength value, see Fig. 9). This feature is a consequence of

Optics EXPRESS

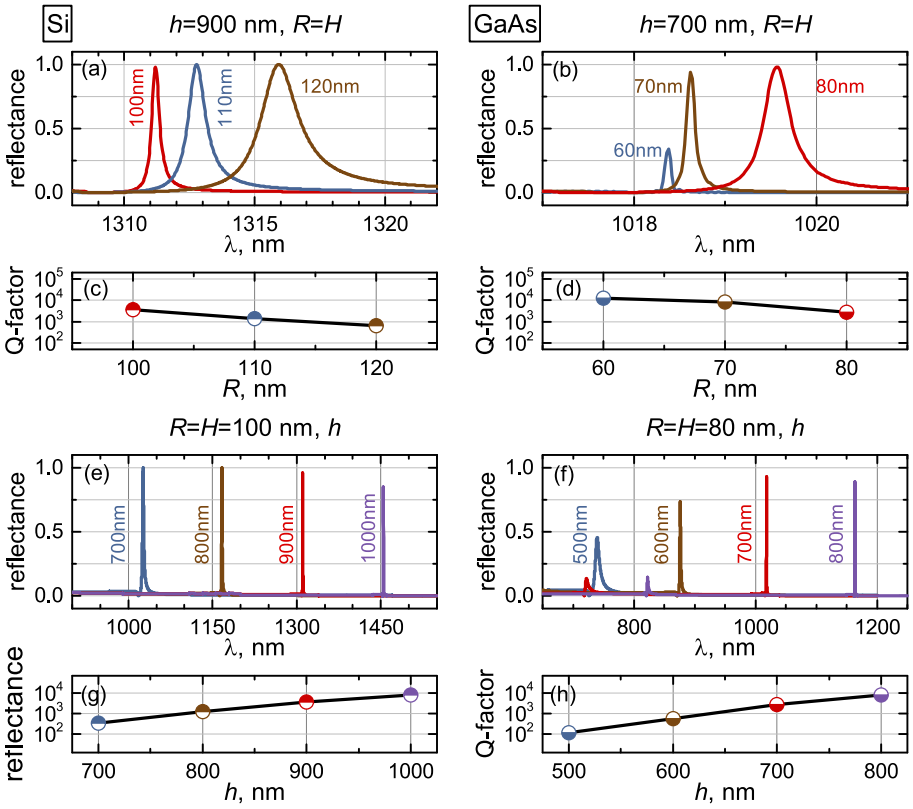

Fig. 7. Reflection spectra for Si (left) and GaAs (right) ND arrays with: (a) fixed h = 900 nm, and for different $R = H$ as shown in legend, (b) fixed h = 700 nm, and for different $R = H$ as shown in legend; (c) and (d) corresponding quality factors of CLRs; (e) fixed $R = H$ = 100 nm and for different h as shown in legend; (f) fixed $R = H$ = 80 nm and for different h as shown in legend; (g) and (h) corresponding quality factors of CLRs.

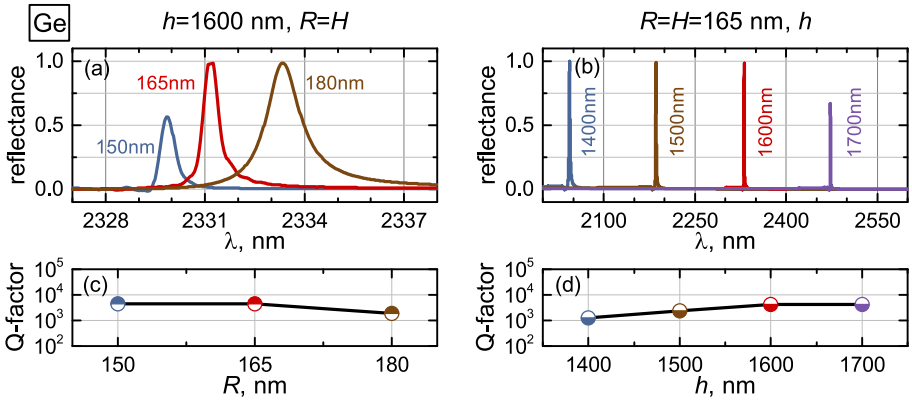

Fig. 8. Reflection spectra for Ge ND arrays with: (a) fixed h = 1600 nm, and for different $R = H$ as shown in legend, (b) fixed $R = H$ = 165 nm and for different h as shown in legend; (c) and (d) corresponding quality factors of CLRs.

Optics EXPRESS

the scale-invariance of Maxwell's equations in the case of non-absorbing and non-dispersive materials. This is the easiest way to predict reflection at a specific wavelength. So if we determine the optimal parameters of the structure (with maximum reflectivity and the CLR Q-factor) by applying the multiplier K to all lattice parameters we can predict the resonance position at any required wavelength. Figures 9(a) and 9(b) show a twofold (for TiO_2 ND array) and 1.5 (for Si ND array) increase in the parameters of the arrays with corresponding shift of the resonance lines, which demonstrates the scale invariance of CLRs. Note, however, that spectra in Fig. 9 are slightly different at various wavelength ranges for the same material due to small variations of the refractive index, as shown in Fig. 2. Nevertheless, scale invariance allows to design and to fabricate optical filters for operation in an arbitrary spectral range from near to far-IR.

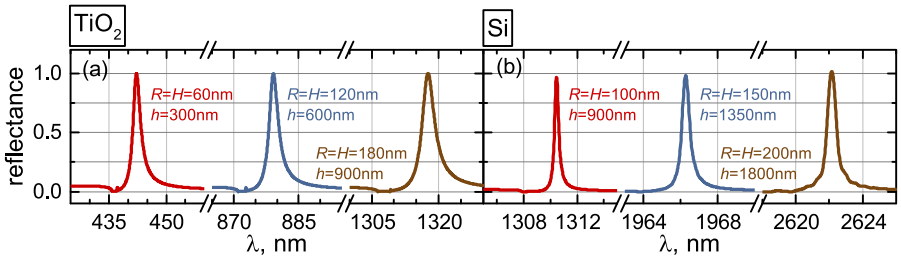

Fig. 9. Reflection spectra for (a) TiO_2 and (b) Si ND arrays with different sizes but with fixed R/H and h/R ratios.

3.3. *Fine tuning the resonance line using the angular dependence of reflection*

The possibility of employing NP arrays for spectral selection of radiation with desired wavelengths in the reflection mode requires deflection of the selected monochromatic radiation away from the incidence direction of the non-monochromatic radiation by tilting the array at least a few degrees. The results of an investigation of this possibility are shown in Fig. 10. It was found that the slope of the array in the range of $1° \le \alpha \le 4°$ is accompanied by a slight decrease in Q-factor of resonance and reflection coefficient. However, the more important effect of this tilting is the shift of the resonance line to the short-wavelength range by about 3 nm when tilting in one plane, and to the long-wavelength range by over 100 nm in another plane. Obviously, the found property of arrays makes it possible to use them for spectral selection and to fine-tune the spectral position of the resonance line to the required wavelength.

Our calculations indicate that at larger angles (α>4°), the resonance shift continues to grow. However, with the increase in the angle up to α>20°, additional resonances with growing amplitude start to emerge at the short-wavelength wing of the CLR, which along with a decrease of the CLR Q-factor impair the selectivity of filtration. To prevent such effects, one should limit the angle to 8–10° or less. Similar results have been obtained for other materials.

Figures 10(c) and 10(d) demonstrate a slight decrease in the CLR Q-factor from $Q = 3.6 \cdot 10^3$ for $\alpha = 0°$ to $Q = 2.9 \cdot 10^3$ and $Q = 10^3$ for $\alpha = 4°$ for TM polarizations, and its increase for TE polarizations with subsequent decrease, respectively. Figure 10 also demonstrates different effects of tilting the array around the Y axis for different polarization of incident radiation. Rotations of the array around the Y axis for TE polarization turn up to be more sensitive to positions of the CLRs than for TM polarization. The explanation of this feature is given considering that the Wood-Rayleigh anomaly in this case follows simple rules. The condition for constructive interference for the case of oblique incidence and square unit cell (the wave vector is in XOZ plane) reads as

$$k_x h = 2\pi p + kh \sin\alpha, \quad k_y h = 2\pi q\,. \tag{2}$$

Optics EXPRESS

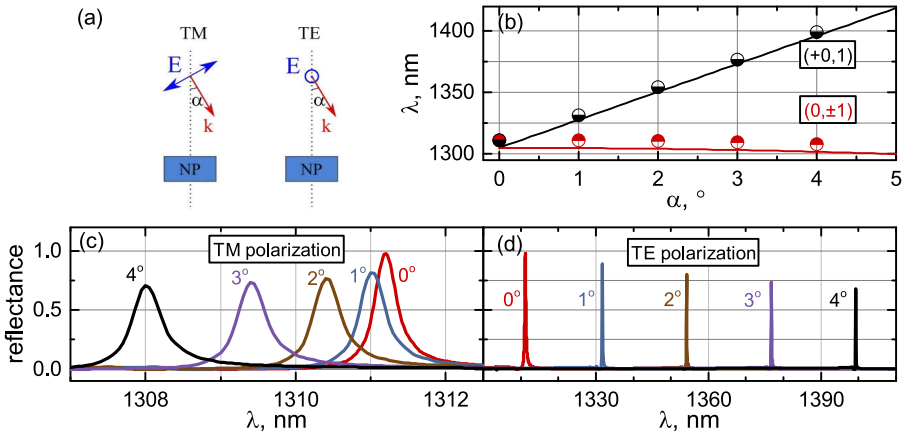

Fig. 10. (a) Sketch of the vector configuration for TM and TE polarization, (b) spectral positions of (+1,0) and (0,±1) Wood-Rayleigh anomalies as a functions of the incidence angle (solid lines) and corresponding positions of reflectance maxima (partially filled circles); The incidence angle dependence of the reflection spectra for Si ND array with h = 900 nm and $R = H$ = 100 nm for (c) TM and (d) TE polarizations.

Here k_x, k_y are x and y components of the scattered wave vector, α is the angle between the wave vector of the incident wave and the Z axis, and k is the absolute value of the wave vector of the incident wave:

$$k = \frac{2\pi n_m}{\lambda} = \sqrt{k_x^2 + k_y^2}\,. \tag{3}$$

For the case of $p = 0$, which corresponds to the TM polarization, we have

$$\lambda = \pm\frac{n_m \cos\alpha}{q} h\,, \tag{4}$$

while for TE polarization ($q = 0$)

$$\lambda = \frac{n_m\,(1 \pm \sin\alpha)}{\pm p} h\,, \tag{5}$$

which describe the angular dependence of the spectral shift for both polarizations. These fast and slow dependencies are shown in Fig. 10(d) and do fully correspond to the spectral features in Figs. 10(a) and 10(b).

Effect of tilting 1D metal-dielectric grating on the position of the CLR spectral line with demonstration of its red shift as the angle of incidence increases was shown in particular in [61], whereas in [43], a blue shift is observed. Our Eqs. (2)–(5) explain this difference. Note that in 1D particle arrays (gratings) [61], the control of position of the extracted spectral line from spectral continuum in the reflection mode with adjustable accuracy by tilting the array in two planes is impossible compared to 2D arrays.

4. Conclusion

Based on the results obtained in this work we can make the following conclusions.

Periodic structures consisting of dielectric highly refractive nanoparticles with low absorption demonstrating collective lattice resonances can be used in the reflection mode as selective ultra-narrowband spectral filters. The position of the spectral lines can be adjusted using the lattice period.

Optics EXPRESS

Arrays with nanoparticles of various shapes (nanodisks and nano-parallelepipeds) demonstrate similar optical properties and can be synthesized by different available experimental techniques.

Dielectric nanoparticle arrays are preferable structures for lossless narrowband reflection compared to plasmonic ones with low refraction and significant absorption of highly conductive materials in the range of the collective lattice resonances.

The geometric parameters of dielectric nanoparticle arrays such as period, size and shape of nanoparticles significantly affect the position of electric dipole resonance in a spectrum and makes it possible to suppress the magnetic dipole resonance as well as to prevent the appearance of several close lines or their splitting in the reflection spectrum instead of a single line that is unacceptable for selective narrow-band filters in the tuning spectral range.

The use of arrays of plasmonic nanoparticles makes it possible to achieve a high-Q CLR response in conditions of strong NP heating (TiN), chemically aggressive media or biological environments (Au, TiN) in spite of a low value of the reflection coefficient. The results obtained indicate that the most suitable material can be determined by taking into account the optical characteristics as well as operating conditions.

Scale invariance of dielectric NPs arrays makes it possible to design and fabricate filters for operation in arbitrary spectral ranges with low dispersion materials from near to far-IR.

The nanoparticle arrays in the reflection mode demonstrate an optical filtering effect with fine tuning of the spectral position of the resonance line to the required wavelength by means of tilting the array with respect to the incident radiation.

The proposed model provides a quantitative interpretation of the angular dependence of the characteristics of a collective lattice resonance for different geometries of the radiation incidence onto the array.

The findings presented in the this work lay the ground for the design and engineering of novel selective tunable optical high-Q filters in a wide range of wavelengths, all the way from the visible down to mid-IR, which are useful for a multitude of applications within applied optics. Various common highly refractive dielectric materials can be used for selecting specific spectral ranges. The criteria for precision in the production of the filters are largely met by contemporary fabrication technology [43,62], making it possible to validate our models and predictions for further fine tuning of the design for special application purposes.

Funding

Russian Science Foundation (18-13-00363); Council on grants of the President of the Russian Federation (075-15-2019-676).

Acknowledgments

The reported study was funded by the Russian Science Foundation, project No. 18-13-00363; the grant of the President of Russian Federation for young scientists No. 075-15-2019-676 (calculations of the electromagnetic field configurations in NPs array).

Disclosures

The authors declare no conflicts of interest.

References

1. M. Meier, P. F. Liao, and A. Wokaun, "Enhanced fields on rough surfaces: dipolar interactions among particles of sizes exceeding the Rayleigh limit," J. Opt. Soc. Am. B **2**(6), 931–949 (1985).
2. K. T. Carron, H. W. Lehmann, W. Fluhr, M. Meier, and A. Wokaun, "Resonances of two-dimensional particle gratings in surface-enhanced Raman scattering," J. Opt. Soc. Am. B **3**(3), 430–440 (1986).
3. S. Zou, N. Janel, and G. C. Schatz, "Silver nanoparticle array structures that produce remarkably narrow plasmon lineshapes," J. Chem. Phys. **120**(23), 10871–10875 (2004).

Optics EXPRESS

4. S. Zou and G. C. Schatz, "Narrow plasmonic/photonic extinction and scattering line shapes for one and two dimensional silver nanoparticle arrays," J. Chem. Phys. **121**(24), 12606–12612 (2004).
5. V. A. Markel, "Divergence of dipole sums and the nature of non-Lorentzian exponentially narrow resonances in one-dimensional periodic arrays of nanospheres," J. Phys. B **38**(7), L115–L121 (2005).
6. B. Auguié and W. L. Barnes, "Collective resonances in gold nanoparticle arrays," Phys. Rev. Lett. **101**(14), 143902 (2008).
7. Y. Chu, E. Schonbrun, T. Yang, and K. B. Crozier, "Experimental observation of narrow surface plasmon resonances in gold nanoparticle arrays," Appl. Phys. Lett. **93**(18), 181108 (2008).
8. V. G. Kravets, F. Schedin, and A. N. Grigorenko, "Extremely narrow plasmon resonances based on diffraction coupling of localized plasmons in arrays of metallic nanoparticles," Phys. Rev. Lett. **101**(8), 087403 (2008).
9. R. W. Wood, "On a remarkable case of uneven distribution of light in a diffraction grating spectrum," Proc. Phys. Soc. Lond. **18**(1), 269–275 (1902).
10. L. Rayleigh, "On the dynamical theory of gratings," Proc. R. Soc. A **79**(532), 399–416 (1907).
11. V. Giannini, G. Vecchi, and J. Gómez Rivas, "Lighting up multipolar surface plasmon polaritons by collective resonances in arrays of nanoantennas," Phys. Rev. Lett. **105**(26), 266801 (2010).
12. A. B. Evlyukhin, C. Reinhardt, U. Zywietz, and B. N. Chichkov, "Collective resonances in metal nanoparticle arrays with dipole-quadrupole interactions," Phys. Rev. B **85**(24), 245411 (2012).
13. M. B. Ross, C. A. Mirkin, and G. C. Schatz, "Optical properties of one-, two-, and three-dimensional arrays of plasmonic nanostructures," J. Phys. Chem. C **120**(2), 816–830 (2016).
14. D. Khlopin, F. Laux, W. P. Wardley, J. Martin, G. A. Wurtz, J. Plain, N. Bonod, A. V. Zayats, W. Dickson, and D. Gérard, "Lattice modes and plasmonic linewidth engineering in gold and aluminum nanoparticle arrays," J. Opt. Soc. Am. B **34**(3), 691–700 (2017).
15. V. I. Zakomirnyi, I. L. Rasskazov, V. S. Gerasimov, A. E. Ershov, S. P. Polyutov, and S. V. Karpov, "Refractory titanium nitride two-dimensional structures with extremely narrow surface lattice resonances at telecommunication wavelengths," Appl. Phys. Lett. **111**(12), 123107 (2017).
16. A. B. Evlyukhin, C. Reinhardt, A. Seidel, B. S. Luk'yanchuk, and B. N. Chichkov, "Optical response features of Si-nanoparticle arrays," Phys. Rev. B **82**(4), 045404 (2010).
17. S. Jahani and Z. Jacob, "All-dielectric metamaterials," Nat. Nanotechnol. **11**(1), 23–36 (2016).
18. S. Liu, M. B. Sinclair, T. S. Mahony, Y. C. Jun, S. Campione, J. Ginn, D. A. Bender, J. R. Wendt, J. F. Ihlefeld, P. G. Clem, J. B. Wright, and I. Brener, "Optical magnetic mirrors without metals," Optica **1**(4), 250–256 (2014).
19. S. Liu, M. B. Sinclair, S. Saravi, G. A. Keeler, Y. Yang, J. Reno, G. M. Peake, F. Setzpfandt, I. Staude, T. Pertsch, and I. Brener, "Resonantly enhanced second-harmonic generation using III–V semiconductor all-dielectric metasurfaces," Nano Lett. **16**(9), 5426–5432 (2016).
20. S. Liu, G. A. Keeler, J. L. Reno, M. B. Sinclair, and I. Brener, "III-V Semiconductor nanoresonators-a new strategy for passive, active, and nonlinear all-dielectric metamaterials," Adv. Opt. Mater. **4**(10), 1457–1462 (2016).
21. V. E. Babicheva and A. B. Evlyukhin, "Resonant lattice Kerker effect in metasurfaces with electric and magnetic optical responses," Laser Photonics Rev. **11**(6), 1700132 (2017).
22. S. Liu, P. P. Vabishchevich, A. Vaskin, J. L. Reno, G. A. Keeler, M. B. Sinclair, I. Staude, and I. Brener, "An all-dielectric metasurface as a broadband optical frequency mixer," Nat. Commun. **9**(1), 2507 (2018).
23. X. Wang, L. C. Kogos, and R. Paiella, "Giant distributed optical-field enhancements from Mie-resonant lattice surface modes in dielectric metasurfaces," OSA Continuum **2**(1), 32–42 (2019).
24. V. I. Zakomirnyi, A. E. Ershov, V. S. Gerasimov, S. V. Karpov, H. Ågren, and I. L. Rasskazov, "Collective lattice resonances in arrays of dielectric nanoparticles: a matter of size," Opt. Lett. **44**(23), 5743–5746 (2019).
25. H. Park and K. B. Crozier, "Multispectral imaging with vertical silicon nanowires," Sci. Rep. **3**(1), 2460 (2013).
26. J. Proust, F. Bedu, B. Gallas, I. Ozerov, and N. Bonod, "All-dielectric colored metasurfaces with silicon Mie resonators," ACS Nano **10**(8), 7761–7767 (2016).
27. Z. Dong, J. Ho, Y. F. Yu, Y. H. Fu, R. Paniagua-Dominguez, S. Wang, A. I. Kuznetsov, and J. K. W. Yang, "Printing beyond sRGB color gamut by mimicking silicon nanostructures in free-space," Nano Lett. **17**(12), 7620–7628 (2017).
28. S. Sun, Z. Zhou, C. Zhang, Y. Gao, Z. Duan, S. Xiao, and Q. Song, "All-dielectric full-color printing with TiO2 metasurfaces," ACS Nano **11**(5), 4445–4452 (2017).
29. S. Enoch, R. Quidant, and G. Badenes, "Optical sensing based on plasmon coupling in nanoparticle arrays," Opt. Express **12**(15), 3422–3427 (2004).
30. R. Adato, A. A. Yanik, J. J. Amsden, D. L. Kaplan, F. G. Omenetto, M. K. Hong, S. Erramilli, and H. Altug, "Ultra-sensitive vibrational spectroscopy of protein monolayers with plasmonic nanoantenna arrays," Proc. Natl. Acad. Sci. **106**(46), 19227–19232 (2009).
31. V. G. Kravets, F. Schedin, A. V. Kabashin, and A. N. Grigorenko, "Sensitivity of collective plasmon modes of gold nanoresonators to local environment," Opt. Lett. **35**(7), 956–958 (2010).
32. N. Bontempi, K. E. Chong, H. W. Orton, I. Staude, D.-Y. Choi, I. Alessandri, Y. S. Kivshar, and D. N. Neshev, "Highly sensitive biosensors based on all-dielectric nanoresonators," Nanoscale **9**(15), 4972–4980 (2017).
33. W. Zhou, M. Dridi, J. Y. Suh, C. H. Kim, D. T. Co, M. R. Wasielewski, G. C. Schatz, and T. W. Odom, "Lasing action in strongly coupled plasmonic nanocavity arrays," Nat. Nanotechnol. **8**(7), 506–511 (2013).
34. S. T. Ha, Y. H. Fu, N. K. Emani, Z. Pan, R. M. Bakker, R. Paniagua-Domínguez, and A. I. Kuznetsov, "Directional lasing in resonant semiconductor nanoantenna arrays," Nat. Nanotechnol. **13**(11), 1042–1047 (2018).

Optics EXPRESS

35. G. Vecchi, V. Giannini, and J. Gómez Rivas, "Shaping the fluorescent emission by lattice resonances in plasmonic crystals of nanoantennas," Phys. Rev. Lett. **102**(14), 146807 (2009).
36. W. Wang, M. Ramezani, A. I. Väkeväinen, P. Törmä, J. G. Rivas, and T. W. Odom, "The rich photonic world of plasmonic nanoparticle arrays," Mater. Today **21**(3), 303–314 (2018).
37. V. G. Kravets, A. V. Kabashin, W. L. Barnes, and A. N. Grigorenko, "Plasmonic surface lattice resonances: a review of properties and applications," Chem. Rev. **118**(12), 5912–5951 (2018).
38. F. J. García de Abajo, R. Gómez-Medina, and J. J. Sáenz, "Full transmission through perfect-conductor subwavelength hole arrays," Phys. Rev. E **72**(1), 016608 (2005).
39. F. J. García de Abajo, "Colloquium: Light scattering by particle and hole arrays," Rev. Mod. Phys. **79**(4), 1267–1290 (2007).
40. W. Zhao, X. Leng, and Y. Jiang, "Fano resonance in all-dielectric binary nanodisk array realizing optical filter with efficient linewidth tuning," Opt. Express **23**(5), 6858–6866 (2015).
41. X. Ma, A. R. James, N. F. Hartmann, J. K. Baldwin, J. Dominguez, M. B. Sinclair, T. S. Luk, O. Wolf, S. Liu, S. K. Doorn, H. Htoon, and I. Brener, "Solitary oxygen dopant emission from carbon nanotubes modified by dielectric metasurfaces," ACS Nano **11**(6), 6431–6439 (2017).
42. F. Shen, Q. Kang, J. Wang, K. Guo, Q. Zhou, and Z. Guo, "Dielectric metasurface-based high-efficiency mid-infrared optical filter," Nanomaterials **8**(11), 938 (2018).
43. R. C. Ng, J. C. Garcia, J. R. Greer, and K. T. Fountaine, "Polarization-independent, narrowband, near-IR spectral filters via guided mode resonances in ultrathin a-Si nanopillar arrays," ACS Photonics **6**(2), 265–271 (2019).
44. B. Auguié, X. M. Bendaña, W. L. Barnes, and F. J. García de Abajo, "Diffractive arrays of gold nanoparticles near an interface: Critical role of the substrate," Phys. Rev. B **82**(15), 155447 (2010).
45. "Lumerical Solutions, "FDTD Solutions", www.lumerical.com/tcad-products/fdtd/".
46. B. D. Thackray, P. A. Thomas, G. H. Auton, F. J. Rodriguez, O. P. Marshall, V. G. Kravets, and A. N. Grigorenko, "Super-narrow, extremely high quality collective plasmon resonances at telecom wavelengths and their application in a hybrid graphene-plasmonic modulator," Nano Lett. **15**(5), 3519–3523 (2015).
47. B. Liang, M. Bai, H. Ma, N. Ou, and J. Miao, "Wideband analysis of periodic structures at oblique incidence by material independent FDTD algorithm," IEEE Trans. Antennas Propag. **62**(1), 354–360 (2014).
48. H. Reddy, U. Guler, Z. Kudyshev, A. V. Kildishev, V. M. Shalaev, and A. Boltasseva, "Temperature-dependent optical properties of plasmonic titanium nitride thin films," ACS Photonics **4**(6), 1413–1420 (2017).
49. P. B. Johnson and R. W. Christy, "Optical constants of the noble metals," Phys. Rev. B **6**(12), 4370–4379 (1972).
50. D. E. Zelmon, D. L. Small, and D. Jundt, "Infrared corrected Sellmeier coefficients for congruently grown lithium niobate and 5 mol% magnesium oxide-doped lithium niobate," J. Opt. Soc. Am. B **14**(12), 3319–3322 (1997).
51. J. R. DeVore, "Refractive indices of rutile and sphalerite," J. Opt. Soc. Am. **41**(6), 416–419 (1951).
52. D. E. Aspnes, S. M. Kelso, R. A. Logan, and R. Bhat, "Optical properties of Al x Ga 1- x As," J. Appl. Phys. **60**(2), 754–767 (1986).
53. D. F. Edwards, "Silicon (Si)," in *Handbook of Optical Constants of Solids*, (Elsevier, 1997), pp. 547–569.
54. R. F. Potter, "Germanium (Ge)," in *Handbook of Optical Constants of Solids*, (Elsevier, 1997), pp. 465–478.
55. N. Bonod and J. Neauport, "Diffraction gratings: from principles to applications in high-intensity lasers," Adv. Opt. Photonics **8**(1), 156–199 (2016).
56. V. S. Gerasimov, A. E. Ershov, A. P. Gavrilyuk, S. V. Karpov, H. Ågren, and S. P. Polyutov, "Suppression of surface plasmon resonance in Au nanoparticles upon transition to the liquid state," Opt. Express **24**(23), 26851–26856 (2016).
57. A. E. Ershov, V. S. Gerasimov, A. P. Gavrilyuk, and S. V. Karpov, "Surface plasmon resonances in liquid metal nanoparticles," Appl. Phys. B **123**(6), 182 (2017).
58. V. S. Gerasimov, A. E. Ershov, S. V. Karpov, A. P. Gavrilyuk, V. I. Zakomirnyi, I. L. Rasskazov, H. Ågren, and S. P. Polyutov, "Thermal effects in systems of colloidal plasmonic nanoparticles in high-intensity pulsed laser fields [Invited]," Opt. Mater. Express **7**(2), 555–568 (2017).
59. I. Staude, A. E. Miroshnichenko, M. Decker, N. T. Fofang, S. Liu, E. Gonzales, J. Dominguez, T. S. Luk, D. N. Neshev, I. Brener, and Y. Kivshar, "Tailoring directional scattering through magnetic and electric resonances in subwavelength silicon nanodisks," ACS Nano **7**(9), 7824–7832 (2013).
60. V. I. Zakomirnyi, S. V. Karpov, H. Ågren, and I. L. Rasskazov, "Collective lattice resonances in disordered and quasi-random all-dielectric metasurfaces," J. Opt. Soc. Am. B **36**(7), E21–E29 (2019).
61. Z. Wang, R. Zhang, and J. Guo, "Quadrupole mode plasmon resonance enabled subwavelength metal-dielectric grating optical reflection filters," Opt. Express **26**(1), 496–504 (2018).
62. D. G. Baranov, D. A. Zuev, S. I. Lepeshov, O. V. Kotov, A. E. Krasnok, A. B. Evlyukhin, and B. N. Chichkov, "All-dielectric nanophotonics: the quest for better materials and fabrication techniques," Optica **4**(7), 814–825 (2017).